Second International Conference on CFD in the Minerals and Process Industries
CSIRO, Melbourne, Australia
6-8 December 1999

SELF-SIMILARITY OF SPATIALLY-DEVELOPING THREE-DIMENSIONAL PLANE WAKES

M. Javad MAGHREBI, Stephen WADE and Julio SORIA

Turbulence Research Laboratory, Dept. Mechanical Engineering
Monash University, Melbourne, Victoria, AUSTRALIA

ABSTRACT

This paper presents a study of the self–similarity of three–dimensional spatially–developing plane wakes. The self–similarity in the near field region of the plane wake flow is addressed with reference to the mean velocity, mean vorticity and second order velocity correlations. The data for this investigation was calculated using a direct numerical simulation of a three–dimensional spatially–developing plane wake.

key words: Self similarity, Wake flow, Spatially developing, Hybrid numerical methods

INTRODUCTION

Self–similar solutions are solutions which depend on a certain combination of the independent variables rather than all of the variables. The hypothesis of self–similarity or self–preservation of the plane wake was first proposed by (Townsend(1956)). Self–similarity in the wake flow is realized if the normalized mean velocity and turbulent statistics (using deficit and wake halfwidth as velocity and length scales) are independent of streamwise location. (Schlichting(1968)) studied the self–similarity of small–deficit plane wakes and introduced a quadratic approximation for the defect velocity. Experiments conducted on unforced, small deficit wakes and in the far region of forced wakes (Corke *et al.* (1992); Marasli *et al.* (1991); Marasli *et al.* (1992); Wygnanski *et al.* (1986)) show that the mean velocity, Reynolds stresses and turbulent intensities are self–preserving. These findings have also been supported in the subsequent temporal simulation of (Ghosal & Rogers(1997)) and the recent direct numerical simulation of temporally–evolving plane wakes by (Moser *et al.* (1998)). However, (Wygnanski *et al.* (1986)) suggested that universal self-similarity does not exist due to the dependency of the normalized mean velocity, length scales, distributions of turbulence intensities and Reynolds stresses on the geometry of wake generators.

An investigation of self–similarity in the near wake region has not been previously performed. This issue is addressed in this paper. This investigation also shows the streamwise location suggesting the start of self–similarity. Four cases using different upstream boundary conditions form the basis for this study.

Case 1 is a wake flow perturbed with a two–dimensional fundamental mode at the forcing frequency of $\omega_f = 0.614$ with a superimposed three–dimensional fundamental mode at the frequency of 0.307. These frequencies correspond to the maximum growth rate for two–dimensional and three–dimensional disturbances, respectively.

Case 2 is a wake flow perturbed with a combination of the two–dimensional fundamental at $\omega_f = 0.614$ and the first subharmonic mode at $\omega_f = 0.307$ superimposed on a three–dimensional fundamental mode at the frequency of 0.307.

Case 3 is a wake flow perturbed with a three–dimensional fundamental mode at a frequency of 0.307 and a combination of two–dimensional fundamental, first subharmonic and second subharmonic modes at the frequencies 0.614, 0.307 and 0.1535, respectively.

Case 4 is a wake flow in which the streamwise velocity component at the inlet boundary is perturbed by a two–dimensional fundamental mode at frequency of 0.614. The cross–stream and spanwise velocity components at the inflow boundary are such that the streamwise vorticity at the inlet boundary of the computational domain is of the following form

$$\omega_1 = 0.1(2 + (2\pi/L_z)^2 - 4y^2)\exp(-y^2)\sin(2\pi z/L_z)$$

The simulation parameters are : $Re = 500$, $N_x = 240$, $N_y = 96$, $N_z = 8$, $U_0(y) = 1 - 0.692\exp(-\ln(2)y^2)$, $L_x = 70$ and $L_z = 8.234$. The simulations were dealiased in y and z directions. The modal amplitude of the forcing functions was set at ten percent of the freestream velocity.

MATHEMATICAL FORMULATION AND NUMERICAL METHOD

The data for this investigation was generated by solving the rotational form of the Navier–Stokes equation for a spatially–developing plane wake. The governing equations, are solved in a domain which is finite in the streamwise direction x, doubly infinite in the cross–stream direction y and homogeneous in the spanwise direction z. In the x direction a high-order compact finite differencing scheme is used. In the y and z directions a mapped spectral method and a Fourier spectral method are used respectively. All quantities are nondimensionalized using the inlet wake halfwidth $b_{1/2}$ and the freestream velocity U_0. The Reynolds number based on these scales is $Re = U_0 b_{1/2}/\nu$. Appropriate manipulation of the Navier–Stokes equations generate the following equations.

$$\frac{\partial \omega}{\partial t} = \nabla \times \mathbf{H} + \frac{1}{Re}\nabla^2 \omega, \qquad (1)$$

$$\frac{\partial \nabla^2 \mathbf{U}}{\partial t} = \nabla \times (\nabla \times \mathbf{H}) + \frac{1}{Re}\nabla^4 \mathbf{U}. \qquad (2)$$

The instantaneous velocity is decomposed into the base flow, the entrainment velocity and the computational variables as indicated by Eqs. (3)–(5).

$$U(x, y, z, t) = u(x, y, z, t) + U_0(y) + xU_e(y) \qquad (3)$$

$$V(x,y,z,t) = v(x,y,z,t) + V_e(y) \quad (4)$$

$$W(x,y,z,t) = w(x,y,z,t) \quad (5)$$

U_e and V_e are the entrainment velocity components and are smooth and continuous functions of y. In all simulations $V_e(y) = -5 \times 10^{-4} \tanh(y)$. $U_e(y)$ and $V_e(y)$ are related such that they satisfy the mass conservation for the entrainment velocity components. Using the streamwise components of Eqs. (1) and (2) and the decomposition shown by Eq. (3) yields:

$$\frac{\partial}{\partial t}\nabla^2 u = \nabla_\perp^2 H_1 - \frac{\partial^2}{\partial x \partial y} H_2 - \frac{\partial^2}{\partial x \partial z} H_3 + \frac{1}{Re}\nabla^4 U, \quad (6)$$

where $\nabla_\perp^2 = \frac{\partial^2}{\partial y^2} + \frac{\partial^2}{\partial z^2}$

$$\frac{\partial}{\partial t}\omega_1 = \frac{\partial}{\partial y} H_3 - \frac{\partial}{\partial z} H_2 + \frac{1}{Re}\nabla^2 \omega_1, \quad (7)$$

Equations. (6), (7) and the convective outflow boundary condition are used for the time–advancement of the simulation. With the help of the continuity equation and the definition of ω_1, the spanwise velocity is obtained by solving

$$\nabla_\perp^2 w = \frac{\partial \omega_1}{\partial y} - \frac{\partial^2 u}{\partial x \partial z}. \quad (8)$$

The cross–stream velocity component v is recovered directly from the continuity equation

$$\frac{\partial v}{\partial y} = -\frac{\partial u}{\partial x} - \frac{\partial w}{\partial z}. \quad (9)$$

Figure 1 shows the coordinate system and the computational domain in which the governing equations for the incompressible plane wake flow are solved. The inlet wake profile is specified by a base flow $U_0(y)$ and the superimposed computational velocity. The wake flow is allowed to develop in x. A uniformly distributed entrainment velocity is specified for v at $\pm\infty$. Boundary conditions for u and

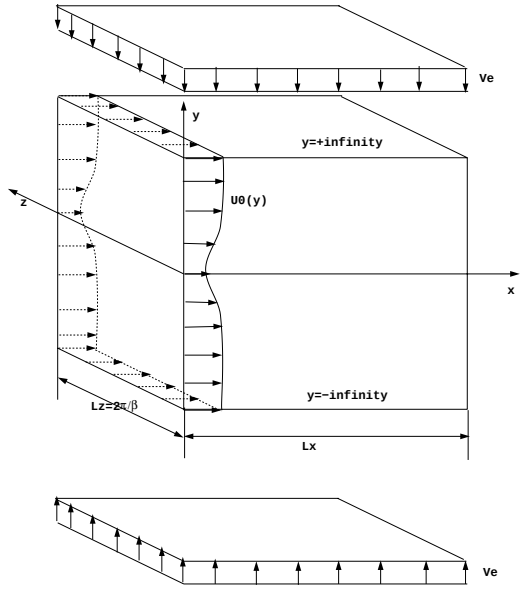

Figure 1: Coordinate system and computational domain.

$\partial u/\partial x$ are specified at the inlet ($x = 0$) and the outlet boundaries ($x = L_x$). The boundary conditions are set to zero in the cross–stream direction. Since the wake flow is assumed to be homogeneous in the z direction, periodic boundary conditions are used in the domain $0 \le z \le L_z$. In the numerical simulations the computational variables at the inlet boundary are specified using a combination of velocity eigenmodes, which are calculated using linear stability analysis, resulting in

$$\begin{aligned}\mathbf{u} = \; & Real[A_{2DF}\hat{\mathbf{u}}_{2DF}(y)\exp(-i\omega_f t) \\ & + A_{2DS}\hat{\mathbf{u}}_{2DS}(y)\exp(-i\omega_f t/2) \\ & + A_{2DSS}\hat{\mathbf{u}}_{2DSS}(y)\exp(-i\omega_f t/4) \\ & + A_{3D}\hat{\mathbf{u}}_{3D}(y) \\ & (\exp(\frac{\beta z - i\omega_f t}{2}) + \exp(\frac{-\beta z - i\omega_f t}{2}))].\end{aligned}$$

Note that the subscripts F, S and SS denote quantities related to fundamental, subharmonic and second subharmonics. Two–dimensional fundamental disturbances are applied in all of the wake simulations. Three–dimensional disturbances, resulting in a pair of oblique waves, are superimposed on the two–dimensional disturbances. This pair has equal and opposite spanwise wavenumbers, chosen such that the angle of the pair of oblique waves is 60°. This is approximately the same as the experimental results of (Meiburg & Lasheras(1987)) which suggest the value of $2/3$ for the ratio of spanwise wavelength to streamwise wavelength. Boundary conditions for Eq. (7) are specified using the definition of ω_1.

Convective boundary conditions of the form :

$$\frac{\partial \mathbf{u}}{\partial t} = -c\frac{\partial \mathbf{u}}{\partial x} \quad (10)$$

are specified at the outflow boundary for all three velocity components. A value of 0.9 was used for c. The boundary conditions must be non–reflective to minimize feedback problems.

An unforced, two–dimensional, wake flow simulation with an inlet mean flow equal to the base profile (Gaussian velocity distribution) provided the initial conditions for the forced wake simulations. A uniformly distributed Gaussian mean velocity profile at all x stations is the initial condition for the unforced two–dimensional wake simulation. All required computations are conducted in physical space in x and in spectral space in y and z. The nonlinear terms are formed by performing the cross product of the velocity and vorticity components in physical space. The products are then transformed back to spectral space where all other computations, including the calculation of the viscous terms in Eqs. (6) and (7), are performed. Exact integration to recover v from the continuity equation introduces constraints which must be satisfied for the entire computational domain at any instant in time. A Galerkin projection was used to satisfy these conditions.

RESULTS AND DISCUSSION

Time averaged statistics of a scalar f, denoted by $\overline{f}$ were performed by averaging f over a time interval. For the cases simulated here, the time interval is determined using the minimum forcing frequency at the inlet of the wake profile ($T = 2\pi/(\omega_f)_{min}$). This is considered to be the appropriate time interval for gathering the statistics when each of the time periods suggested by the different forcing frequencies is an integer factor of the smallest time period ($T = 2\pi/(\omega_f)_{max}$). Otherwise, mean statistics of the

samples ($\overline{f}$) are obtained by using a long time period for collecting the samples. This approach was tested by comparing first and second order velocity correlations using long time averaging and one time period averaging, resulting in identical results (**?**). Statistics [1] relating to the velocity components of three–dimensional simulations are also averaged over the homogeneous direction (z), this ensemble average operator being denoted by "<>". Successive application of the ensemble and time average operators form the ensemble mean operator which is defined by:

$$< \overline{f} >= \frac{\int_0^{L_z} \int_{t_0}^{t_0+T} f(z,t)\,dz dt}{T.L_z}$$

Prior to any sampling of data for statistical analysis, it is ensured that the initial conditions for either unforced or forced simulation have been washed out of the computational domain.

The first order spanwise vorticity and the first and second order velocity correlations, which are ensemble averaged, are scaled using the local halfwidth and the velocity deficit at different streamwise locations. These quantities are investigated to ascertain self–similarity. Figure 2 shows the streamwise velocity profiles in self–similar coordinates for Cases 1 to 4.

This data shows self–similarity in the core region of the plane wake and in the vicinity of the freestream. The velocity profiles in the other regions of the plane wake show a small deviation in self–similarity coordinates. The deviations are less noticeable as the wake develops in the streamwise direction. The velocity profiles at the last two streamwise locations are almost identical. In other words, self–similarity of the mean streamwise velocity is approached as the wake develops downstream. Around the streamwise location of $x = 50$, self–similarity can be detected for the mean streamwise velocity profiles.

The mean spanwise vorticity was also examined for evidence of self–similarity. The vorticity distribution of the wake flow in self–similar coordinates where the vorticity and the cross–stream distance are normalized by $\Delta U_c / b_{1/2}(x)$ and $b_{1/2}$ respectively are shown in Fig. 3. The data indicates that the spanwise vorticity profiles for the near field region of the wake flow in the vicinity of the wake center and in the freestream regions are self–similar. Like the streamwise velocity profiles, the self–similarity of the vorticity profiles becomes more evident as the wake develops downstream.

The start of self–similarity in the velocity and vorticity profiles can be related to the location where the ensemble average of the centerline velocity and the wake halfwidth are constant. For the wake flows concerned, this was detected at approximately $x = 50$, which is consistent with the results shown earlier.

The second order velocity correlations (turbulence intensities) are presented in Figs. 4 through 6. The data in these figures show only little self–similarity at any stages of the wake development. Only at the last two streamwise locations do the profiles approach the same general shape. The distribution of the profiles also indicate the collapse of the profiles in that regions. Other velocity correlations (first or second order) which are not presented here do not exhibit self–similarity.

[1] No statistical information was gathered in the vicinity of the outflow boundary conditions.

CONCLUSION

Numerical simulations of a spatially–developing three–dimensional plane wake flow has been performed. Different upstream environments have been used to investigate the self–similarity characteristics of this flow. The first order statistics for the streamwise velocity and spanwise vorticity components show that the profiles are self–similar in the center region and in the freestream regions of the wake flows. In general the collapse of these profiles is reasonably good for the entire domain. The square root of the second order velocity correlation are found to be symmetric about $y = 0$. These profiles were not self–similar in the early stages of the wake development but the distributions show a similar shape and self–similarity becomes more evident as the wake develops further downstream. The ensemble average of the streamwise velocity and spanwise vorticity profiles are approximately self–similar in the far downstream region of the wake. The profiles in the near wake region show self–similarity in the vicinity of the wake centerline and near the freestream boundaries.

ACKNOWLEDGEMENTS

The first author gratefully acknowledges the grant of scholarship awarded by the Ministry of Culture and Higher Education of Iran. The support of an ARC grant is also acknowledged.

REFERENCES

CORKE, T. C., KRULL, J. D., & GHASSEMI, M. (1992). Three–Dimensional Mode Resonance in Far Wakes. *J. Fluid Mech.* **239**, 99–132.

GHOSAL, S. & ROGERS, M. M. (1997). A Numerical Study of Self–similarity in a Turbulent Plane Wake Using Large Eddy Simulation. *Phys. Fluids* **9**(6), 1729–1739.

MARASLI, B., CHAMPAGNE, F. H., & WYGNANSKI, I. (1991). On Linear Evolution of Unstable Disturbances in a Plane Turbulent Wake. *Physics of Fluids A* **3**(4), 665–674.

MARASLI, B., CHAMPAGNE, F. H., & WYGNANSKI, I. (1992). Effect of Travelling Waves on the Growth of a Plane Turbulent Wake. *J. Fluid Mech.* **235**, 511–528.

MEIBURG, E. & LASHERAS, J. C. (1987). Comparison between Experiments and Numerical Simulations of Three–Dimensional Plane Wakes. *Phys. Fluids* **30**(3), 623–625.

MOSER, R. D., ROGERS, M. M., & EWING, D. W. (1998). Self–Similarity of Time–Evolving Plane Wakes. *J. Fluid Mech.* **367**, 255–289.

SCHLICHTING, H. (1968). *Boundary Layer Theory*. McGrow–Hill.

TOWNSEND, A. A. (1956). *The Structure of Turbulent Shear Flow*. Cambridge University Press.

WYGNANSKI, I. J., CHAMPAGNE, F., & MARASLI, B. (1986). On the Large Scale Structures in Two–Dimensional, Small–Deficit, Turbulent Wakes. *J. Fluid Mech.* **168**, 31–71.

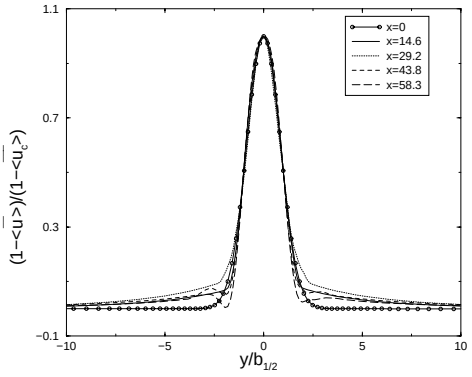

(a)

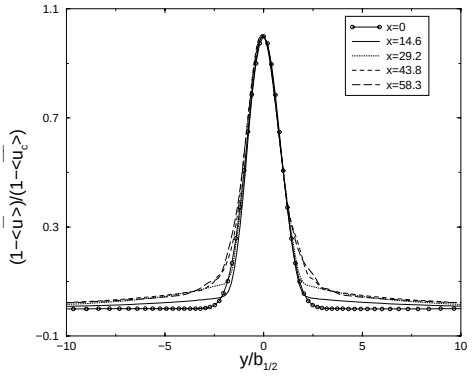

(b)

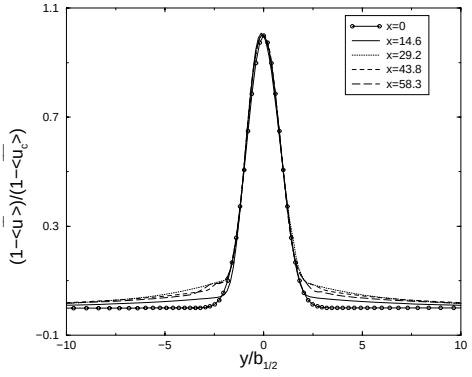

(c)

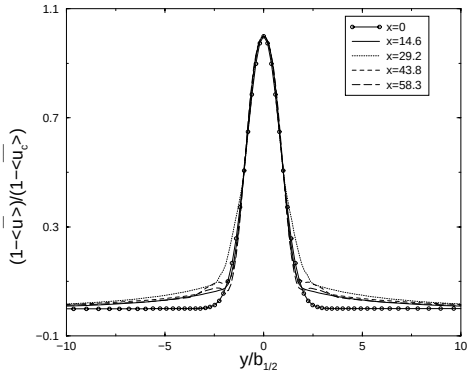

(d)

Figure 2: Profiles of $(1- < \overline{u} >)/(1- < \overline{U_c} >)$, at different downstream distances in self–similar coordinates: (a) Case 1, (b) Case 2, (c) Case 3, (d) Case 4.

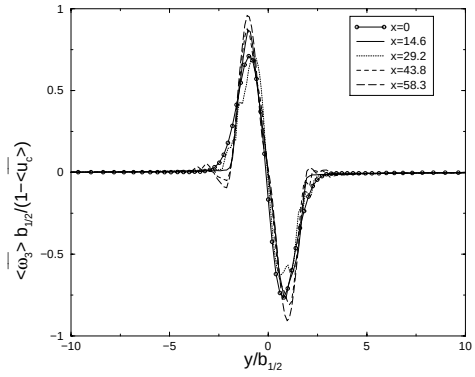

(a)

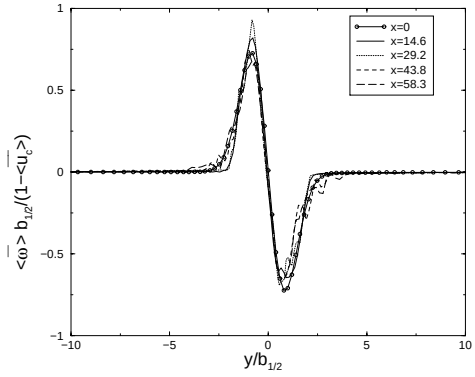

(b)

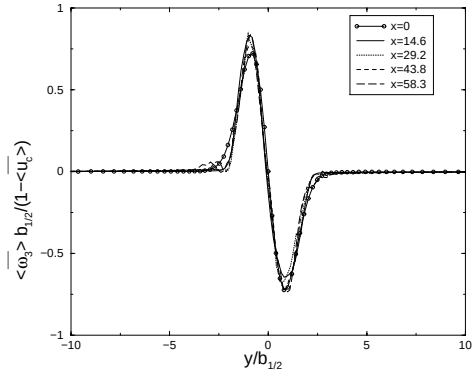

(c)

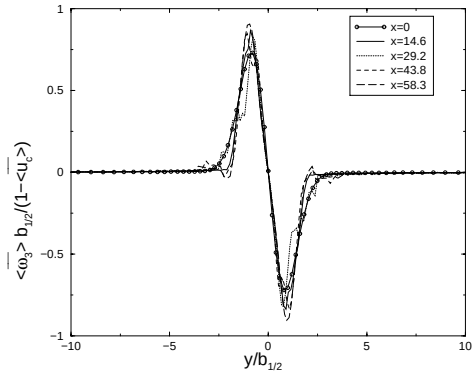

(d)

Figure 3: Profiles of $< \overline{\omega_3} >< \overline{b_{1/2}} > /(1- < \overline{U_c} >)$ at different downstream distances in self–similar coordinates: (a) Case 1, (b) Case 2, (c) Case 3, (d) Case 4.

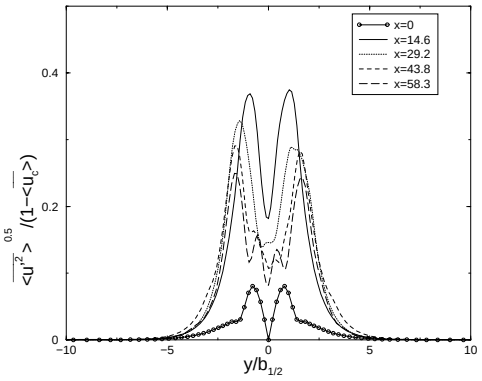

(a)

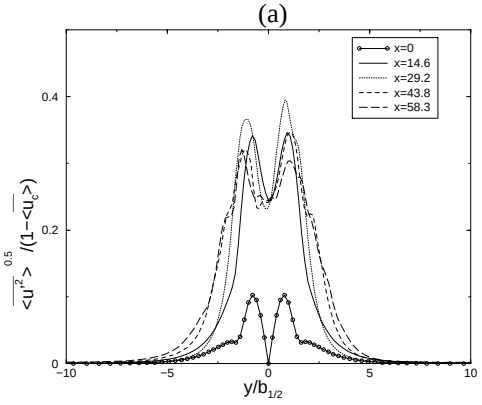

(b)

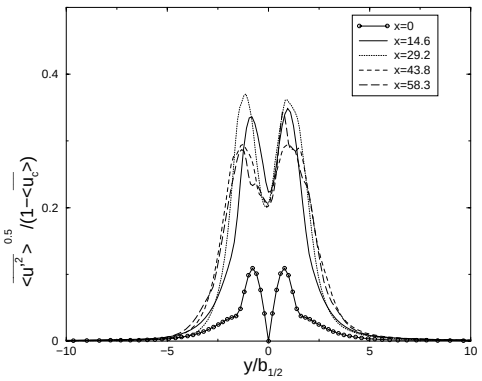

(c)

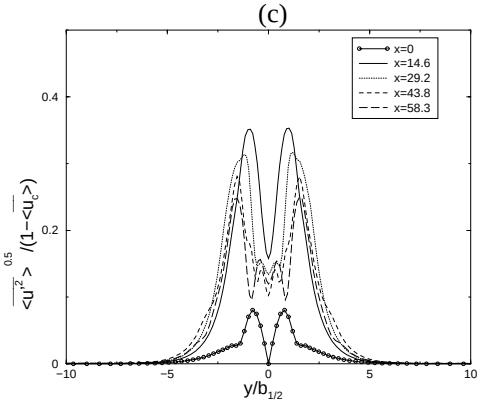

(d)

Figure 4: Normalized turbulence intensity profiles, $\sqrt{\overline{u'^2}}$,at different downstream distances in self–similar coordinates: (a) Case 1, (b) Case 2, (c) Case 3, (d) Case 4

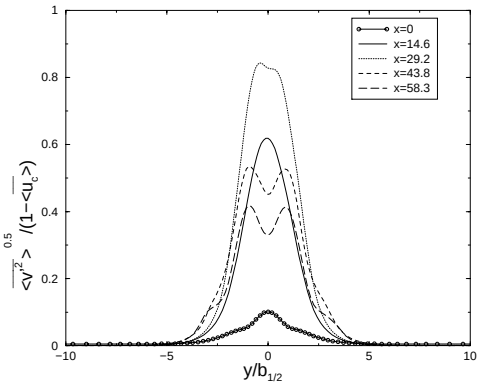

(a)

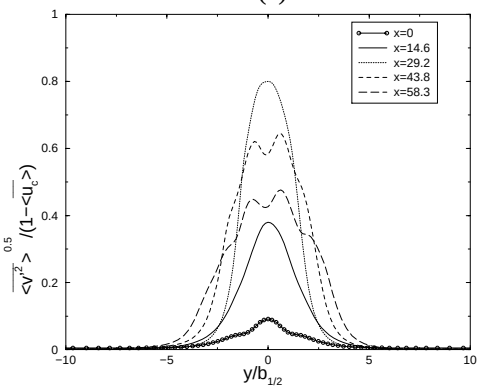

(b)

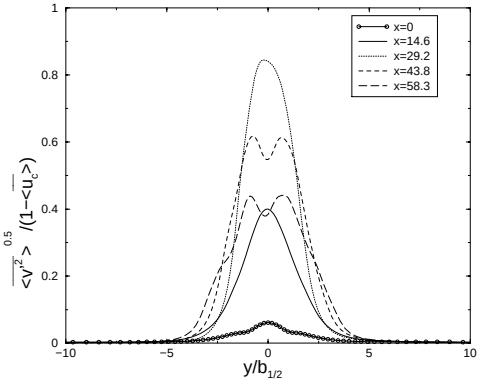

(c)

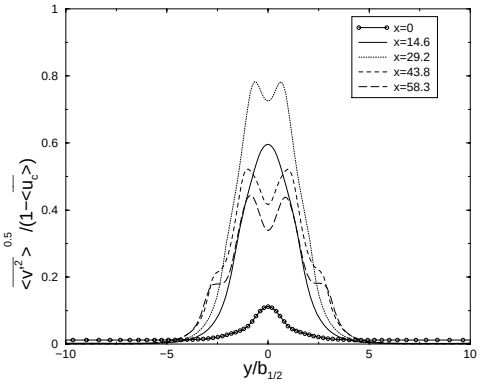

(d)

Figure 5: Normalized turbulence intensity profiles, $\sqrt{\overline{v'^2}}$,at different downstream distances in self–similar coordinates: (a) Case 1, (b) Case 2, (c) Case 3, (d) Case 4

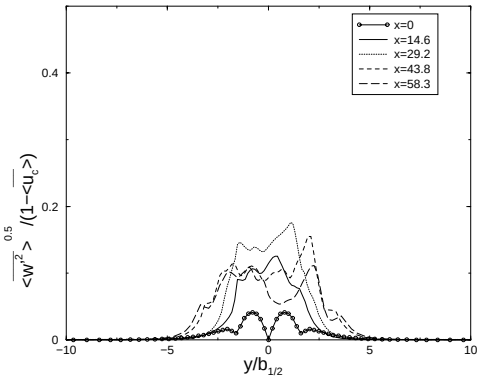

(a)

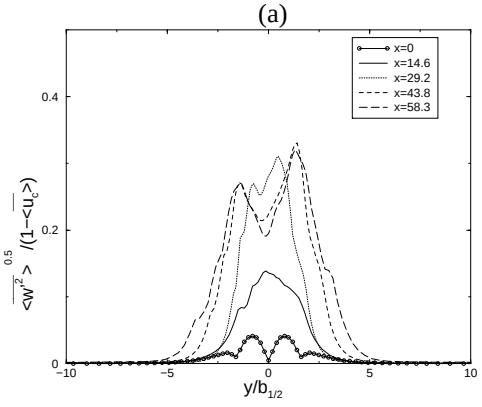

(b)

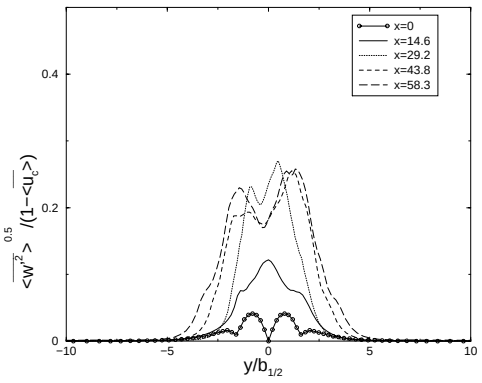

(c)

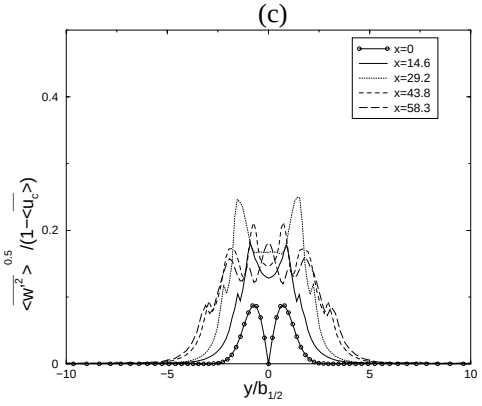

(d)

Figure 6: Normalized turbulence intensity profiles, $\sqrt{\overline{w'^2}}$,at different downstream distances in self–similar coordinates: (a) Case 1, (b) Case 2, (c) Case 3, (d) Case 4